




## Combined electric and photocontrol of selective light reflection at an oblique helicoidal cholesteric liquid crystal doped with azoxybenzene derivative

Kamal Thapa,<sup>1,2</sup> Olena S. Iadlovska,<sup>1,2</sup> Hari Krishna Bisoyi <sup>1</sup>, Daniel A. Paterson,<sup>3</sup> John M. D. Storey,<sup>3</sup> Corrie T. Imrie,<sup>3</sup> Quan Li,<sup>1,4</sup> Sergij V. Shiyonovskii <sup>1,4</sup> and Oleg D. Lavrentovich <sup>1,2,4,\*</sup>

<sup>1</sup>Advanced Materials and Liquid Crystal Institute, Kent State University, Kent, Ohio 44242, USA

<sup>2</sup>Department of Physics, Kent State University, Kent, Ohio 44242, USA

<sup>3</sup>Department of Chemistry, School of Natural and Computing Sciences, University of Aberdeen, AB24 3UE Scotland, United Kingdom

<sup>4</sup>Materials Science Graduate Program, Kent State University, Kent, Ohio 44242, USA



(Received 25 July 2021; accepted 16 September 2021; published 13 October 2021)

An oblique helicoidal cholesteric liquid crystal  $\text{Ch}_{\text{OH}}$  represents a unique optical material with a single-harmonic periodic modulation of the refractive index and a pitch that can be tuned by an electric or magnetic field in a broad range from submicrometers to micrometers. In this work, we demonstrate that the oblique helicoidal cholesteric doped with azoxybenzene molecules can be tuned by both the electric field and light irradiation. The tuning mechanism is explained by the kinetics of *trans-cis* photoisomerization of the azoxybenzene molecules. At a fixed voltage, UV irradiation causes a redshift of the reflection peak by more than 200 nm. The effect is caused by an increase of the bend elastic constant of  $\text{Ch}_{\text{OH}}$  under irradiation. The demonstrated principle has the potential for applications such as smart windows, sensors, tunable lasers, and filters.

DOI: [10.1103/PhysRevE.104.044702](https://doi.org/10.1103/PhysRevE.104.044702)

### I. INTRODUCTION

Cholesteric (Ch) liquid crystals (LCs) are composed of chiral molecules that arrange into a twisted structure, forming a right-angle helicoid. The molecules align perpendicularly to the twist axis. When the Ch pitch  $P$  is in the submicrometer range, a uniformly aligned Ch shows a selective reflection of light in the visible spectral range. For unpolarized light propagating along the Ch helical axis, the circularly polarized component of light with the same handedness as the Ch is reflected, and the opposite handedness is transmitted. The selective Bragg reflection's peak wavelength  $\lambda_P = \bar{n}P$  and its bandwidth  $\Delta\lambda = \Delta nP$  are defined by the pitch  $P$ , average value  $\bar{n} = (n_e + n_o)/2$  of extraordinary  $n_e$  and ordinary  $n_o$  refractive indices, and birefringence  $\Delta n = n_e - n_o$  [1]. The wavelength of the reflected light can be controlled by temperature, chemical compositions, and by the concentration of chiral dopants since these could change both the refractive indices and the pitch  $P$ . However, the most desirable electromagnetic mode to control light diffraction by Ch has been elusive. The reason is that the applied field either does not change the pitch or destroys the single-harmonic modulation of the refractive indices [2,3], thus reducing the efficiency of diffraction [4–6]. If the dielectric or diamagnetic anisotropy is negative, the director and the Ch pseudolayers align perpendicularly to the field and there is no torque that could change the pitch. If the anisotropy is positive, the helical axis aligns perpendicularly to the applied field. In this state, the regions in which the director is parallel to the field expand at the expense of the regions in which the director must be perpendicular to the field [2–5]. Although the pitch grows with the field, the

uniform rate of twist is lost. The helical structure distorted by the field is no longer of a single-harmonic character and efficiency of the light diffraction is diminished, as demonstrated experimentally for various geometries, with the Ch axis in the plane of the cell [4,5] or normal to it [6].

Recent developments in the synthesis of mesomorphic compounds in the form of flexible dimers that show an anomalously low value of the bend elastic constant  $K_{33}$  led to the realization of an oblique helicoidal cholesteric ( $\text{Ch}_{\text{OH}}$ ) state, in which the director twists around the helical axis while remaining tilted rather than perpendicular to it [7,8]. The stability of this  $\text{Ch}_{\text{OH}}$  state, which contains both twist and bend director deformations, requires the bend elastic constant  $K_{33}$  to be smaller than the twist  $K_{22}$  modulus, as predicted theoretically by de Gennes [2] and Meyer [3]. When an electric  $\mathbf{E}$  [7,8] or magnetic  $\mathbf{H}$  [9] field acts along the  $\text{Ch}_{\text{OH}}$  axis, it changes the conical angle  $\theta$  of the director and the pitch of the structure but does not modify the single-harmonic character of the twist. For optical applications, it means that the efficiency of light reflection remains high in the entire range of pitch values controlled by the field. In a single  $\text{Ch}_{\text{OH}}$  cell, the wavelength of reflected (or transmitted) light can be tuned in a very broad range, from UV to near IR [8,9]. The  $\text{Ch}_{\text{OH}}$  structure is also sensitive to the torques induced by the electromagnetic field of light, which allows one to control the pitch by combining the low-frequency electric field [7,8] and the electromagnetic field at optical frequencies [10].

The responsiveness of Ch could be extended to photochemical effects by doping the chiral mixtures with photoresponsive molecules capable of photoisomerization. In the well-known phenomenon of *trans-to-cis* isomerization of azobenzenes and azoxybenzenes, light irradiation in the UV and visible parts of the spectrum changes the molecular shapes and interactions and affects the Ch pitch and the

\*olavrent@kent.edu

refractive indices, and hence the wavelength and bandwidth of selective Bragg reflection [11–18]. In various embodiments, photocontrol could be achieved by doping a Ch with a photosensitive achiral material [11], by using a photosensitive nematic as a host for Ch with a nonphotosensitive chiral dopant [15,19–22], and by using a photosensitive chiral dopant [12,16,17,23–31]; see the recent reviews [32–34]. Photocontrol of Ch can be used to fabricate optical filters with tunable wavelength and bandwidth [35] and optically tunable lasers [36]. A UV control of optical transparency at longer wavelengths, in near IR, can potentially be of interest in the development of smart windows [37].

In this work, we demonstrate experimentally that a combined action of the electric field and UV irradiation could continuously tune the  $\text{Ch}_{\text{OH}}$  pitch and the wavelength of selective reflection of light with longer wavelengths, in the visible part of the spectrum and potentially far beyond. To achieve the dual electric and photocontrol, the  $\text{Ch}_{\text{OH}}$  composition is prepared with flexible dimers and doped with a photosensitive achiral *p*, *p'*-diheptylazoxybenzene (D7AOB), which experiences *trans*-to-*cis* isomerization under UV irradiation and reverse transition under thermal relaxation [38], similarly to its azobenzene counterpart *p*, *p'*-diheptylazobenzene [39]. The maximum absorbance of D7AOB is at 340 nm and then decays as the wavelength of irradiation increases [38]. The presence of flexible dimers in the mixtures guarantees the smallness of  $K_{33}$  [40,41]. At a fixed voltage, UV irradiation causes a gradual redshift of the reflection wavelength by about 235 nm for the explored composition. A unique feature of  $\text{Ch}_{\text{OH}}$  is a well-defined relationship between the material parameters such as elastic moduli, birefringence, and pitch. Using this relationship, we demonstrate that the main reason for the UV-induced redshift of the Bragg reflection wavelength is the increase of  $K_{33}$ . The dynamic scenarios of the irradiation-induced changes are described by kinetic equations. The combined action of the electric field and UV irradiation in the  $\text{Ch}_{\text{OH}}$  doped with D7AOB can find applications in smart windows, lasers, and optical filters, as well as in sensors for measuring UV intensities and doses.

## II. MATERIALS AND METHODS

The photosensitive  $\text{Ch}_{\text{OH}}$  mixture contains a rodlike mesogen pentylcyanobiphenyl (5CB); photosensitive azoxybenzene derivative *p*, *p'*-diheptylazoxybenzene (D7AOB, Fig. 1) which is also a mesogen in its pure form [42–44]; flexible dimers 1'',7''-bis(4-cyanobiphenyl-4'-yl) heptane (CB7CB) and 1-(4-cyanobiphenyl-4'-yloxy)-6-(4-cyanobiphenyl-4'-yl) hexane (CB6OCB); and left-handed chiral dopant S811 (EM Industries), in the following weight proportion: 5CB:D7AOB:CB7CB:CB6OCB:S811 = 42.0:10.0:28.5:15.5:4.0. The mixture shows a transition from an isotropic (I) to a chiral nematic ( $\text{N}^*$ ) phase at  $T_{\text{I-N}^*} = 64.4^\circ\text{C}$  and from  $\text{N}^*$  to a chiral analog of the twist-bent nematic ( $\text{N}_{\text{TB}}$ ) phase at  $T_{\text{N}^*-\text{N}_{\text{TB}}} = 22.0^\circ\text{C}$ . The flexible dimers CB7CB and CB6OCB reduce the bend elastic constant  $K_{33}$ , while other components help to keep the temperature range of a small  $K_{33}$  close to the room temperature; small  $K_{33}$  assures the stability of the  $\text{Ch}_{\text{OH}}$  state. Note that the photosensitive mesogenic dopant D7AOB shows a relatively small  $K_{33}$  in

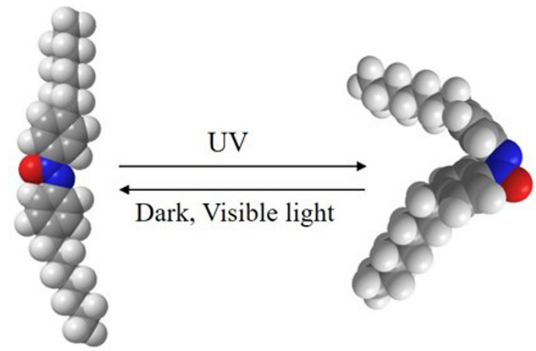


FIG. 1. *Trans* and *cis* isomers of D7AOB molecule.

its nematic phase well above the transition temperature to the smectic-*A* phase [44].

The cells are assembled from two indium tin oxide (ITO) patterned glass substrates. One plate is spin coated with a polyimide, PI2555, and rubbed unidirectionally to achieve planar alignment. The other plate is coated with a silicone elastomer, SE5661, for homeotropic surface anchoring; see Fig. 2. The planar plate helps to stabilize the structure, while the homeotropic substrate allows a continuous (as opposed to stepwise) variation of the pitch and the reflection wavelength of  $\text{Ch}_{\text{OH}}$ .

The thickness of the cells is set by spherical spacers mixed with UV-curing adhesive NOA68 (Norland Products, Inc.) and measured by the interferometric technique using a Lambda 18 UV/VIS spectrometer (PerkinElmer, Inc). The cells are filled with the  $\text{Ch}_{\text{OH}}$  mixture in the isotropic phase through capillary force action.

A sinusoidal ac voltage with a frequency 3 kHz is applied to 5 mm  $\times$  5 mm ITO electrodes of the  $\text{Ch}_{\text{OH}}$  cells using a DS345 waveform generator (Stanford Research) and a 7602M voltage amplifier (KROHN-HITE Co.). The selective reflection spectra are observed using a tungsten halogen light source, LS-1, with a working range 360–2000 nm and a USB2000 fiber optics spectrometer (both Ocean Optics, Co.). An unpolarized light beam from LS-1 is passed through a UV-VIS bifurcated fiber (200  $\mu\text{m}$  diameter) and focused by the lens into a paraxial ray incident normally at the planar surface of the  $\text{Ch}_{\text{OH}}$  cells. The superimposed reflected beam is passed back through the bifurcated fiber and detected by a USB2000 spectrometer interfaced with Oceanview spectroscopy software (Ocean Optics, Co.). The light source LS-1 is switched on throughout the entire experiment. In the experiments in

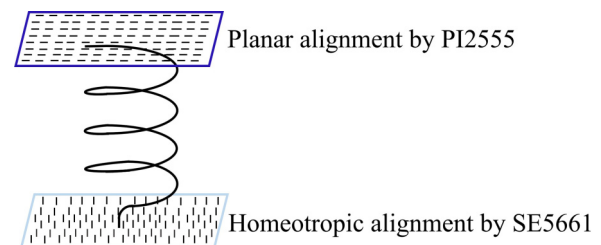


FIG. 2. A schematic representation of hybrid surface anchoring in a  $\text{Ch}_{\text{OH}}$  cell.

which the UV irradiation is absent, to avoid potential photoisomerization caused by LS-1, a broadband filter is placed on the cells to cut off the light of wavelengths below 450 nm.

An LED lamp, M365LP1, with an emission wavelength at 365 nm is used as a UV light source, and the light intensity is measured by an S170C power meter (both Thorlabs, Inc.). To separate the photochemical and dielectric heating effects from the UV-induced thermal effects, the temperature of the samples during UV and electric field activation is measured by a thermocouple (accuracy 0.01 °C) attached to the glass plate of the cell.

The material properties important for the analysis of the UV effect are the dielectric anisotropy  $\Delta\varepsilon = \varepsilon_{\parallel} - \varepsilon_{\perp}$ , where  $\varepsilon_{\parallel}$  and  $\varepsilon_{\perp}$  are the parallel and perpendicular components of dielectric permittivity, extraordinary  $n_e$  and ordinary  $n_o$  refractive indices, and, most importantly, the bend modulus  $K_{33}$ . These parameters were measured before UV exposure and after 1.5 h under continuous UV exposure.

The dielectric permittivities are derived from the capacitance measurements in the planar  $\text{Ch}_{\text{OH}}$  cell under an applied field with the frequency 3 kHz using an LCR meter 4284A (Hewlett Packard). The perpendicular component  $\varepsilon_{\perp}$  is determined at a low voltage that does not perturb the planar structure and  $\varepsilon_{\parallel}$  is measured by applying a high voltage that unwinds the  $\text{Ch}_{\text{OH}}$  state into a homeotropic N state [41].

The refractive indices are measured in the wedge cell filled with the nematic analog of the  $\text{Ch}_{\text{OH}}$  mixture using an interference technique [45]. The nematic mixture has the same concentration of D7AOB as the  $\text{Ch}_{\text{OH}}$  mixture, 5CB:D7AOB:CB7CB:CB6OCB = 41.8:10.0:31.3:16.9 ( $T_{I-N} = 75.1^\circ\text{C}$ ,  $T_{N-N_{\text{TB}}} = 19.4^\circ\text{C}$ ). The cell with a small wedge angle 0.00675 rad is assembled from two planar ITO-PI 2555 glass substrates with the rubbing direction perpendicular to the thickness gradient, in order to avoid director deformations. The measurements are performed at three different wavelengths, 432, 532, and 632.8 nm, using laser line color filters with 1 nm central bandwidth (Thorlabs, Inc.). The thickness of the thick end of the wedge is fixed by 100  $\mu\text{m}$  spacers mixed with adhesive NOA68; there are no spacers at the glued wedge end.

The bend elastic constant  $K_{33}$  is measured in the hybrid  $\text{Ch}_{\text{OH}}$  cell using the dependence of the Bragg reflection wavelength  $\lambda_P$  on the applied electric field  $E$  [41],  $\lambda_P/n_o(\lambda_P) = a_1E^{-1} + a_2E^{-2}$ , where the ordinary refractive index should be evaluated at the corresponding wavelength,  $n_o = n_o(\lambda_P)$ ;  $a_1$  and  $a_2$  are the fitting parameters. Using the three measured values of the ordinary refractive index, we find the polynomial coefficients of the Cauchy dispersion relation  $n_o(\lambda) = A + B\lambda^{-2} + C\lambda^{-4}$  and calculate the ratio  $\lambda_P/n_o(\lambda_P)$ . The field dependency of  $\lambda_P/n_o(\lambda_P)$  is fitted with a polynomial  $a_1E^{-1} + a_2E^{-2}$  to find  $a_1$  and  $a_2$ . The slope  $a_1 = 2\pi\sqrt{\frac{K_{33}}{\varepsilon_o\Delta\varepsilon}}$  is used to determine  $K_{33}$ ; the correction  $a_2E^{-1}$  is negligibly small as compared to  $a_1$ . Similar results were obtained for other  $\text{Ch}_{\text{OH}}$  materials; see Ref. [41].

### III. RESULTS AND DISCUSSION

We start by presenting the known features of the field response of  $\text{Ch}_{\text{OH}}$  [7,8,41,46–48]. The balance of anisotropic

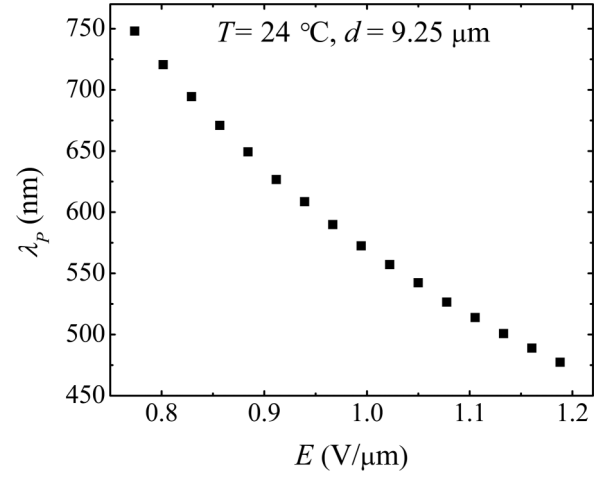


FIG. 3. Electric field dependence of the peak wavelength  $\lambda_P$  measured at the planar side of the hybrid  $\text{Ch}_{\text{OH}}$  cell with thickness  $d = (9.25 \pm 0.02) \mu\text{m}$  at temperature  $T = 24.0^\circ\text{C}$ .

dielectric coupling to the field, twist, and bend elastic energies establishes the following field dependencies of the  $\text{Ch}_{\text{OH}}$  pitch  $P$  [2,3],

$$P = \frac{2\pi}{E} \sqrt{\frac{K_{33}}{\varepsilon_o\Delta\varepsilon}}, \quad (1)$$

and the conical angle  $\theta$  that the director  $\hat{\mathbf{n}}$  makes with the helicoidal axis [7],

$$\sin^2\theta = \frac{K_{33}}{K_{22} - K_{33}} \left( \frac{E_{\text{NC}}}{E} - 1 \right), \quad (2)$$

where  $E_{\text{NC}} = \frac{2\pi K_{22}}{P_o\sqrt{\varepsilon_o\Delta\varepsilon K_{33}}}$  is a critical field, typically in the range (3–5) V/ $\mu\text{m}$ , above which  $\text{Ch}_{\text{OH}}$  unwinds into a state with the director along the field,  $\theta = 0^\circ$ ;  $P_o$  is the intrinsic pitch of Ch in the absence of field. The electrically controlled periodic structure of  $\text{Ch}_{\text{OH}}$  reflects normally incident light within a band gap  $[n_oP, n_{e,\text{eff}}P]$  with the central wavelength

$$\lambda_P = \bar{n}_{\text{eff}}P = \frac{(n_o + n_{e,\text{eff}})P}{2}, \quad (3)$$

where  $n_{e,\text{eff}} = n_o n_e / \sqrt{n_e^2 \cos^2\theta + n_o^2 \sin^2\theta}$  is the effective value of the extraordinary refractive index that depends on the conical angle  $\theta$ .

The field dependence of the selective Bragg reflection of light by the studied mixture in the absence of UV irradiation is shown in Fig. 3. It is measured in a hybrid cell of the thickness  $d = (9.25 \pm 0.02) \mu\text{m}$  at a constant temperature  $T = T_{N^*-N_{\text{TB}}} + 2^\circ\text{C} = 24^\circ\text{C}$ . The peak wavelength  $\lambda_P$  is calculated as the coordinate of the middle of the width at the half amplitude of the Bragg peak. The field is first raised to 4.0 V/ $\mu\text{m}$  above  $E_{\text{NC}}$ , at which the Ch is completely unwound and the director is aligned uniformly along the electric field and then reduced to form  $\text{Ch}_{\text{OH}}$  and to measure the reflection spectra. The electric field that tunes Bragg reflection in the visible part of the spectrum is relatively weak, only (0.8–1.2) V/ $\mu\text{m}$ ; see Fig. 3.

To explore whether the UV irradiation could independently control the structural color of  $\text{Ch}_{\text{OH}}$ , we used the same cell

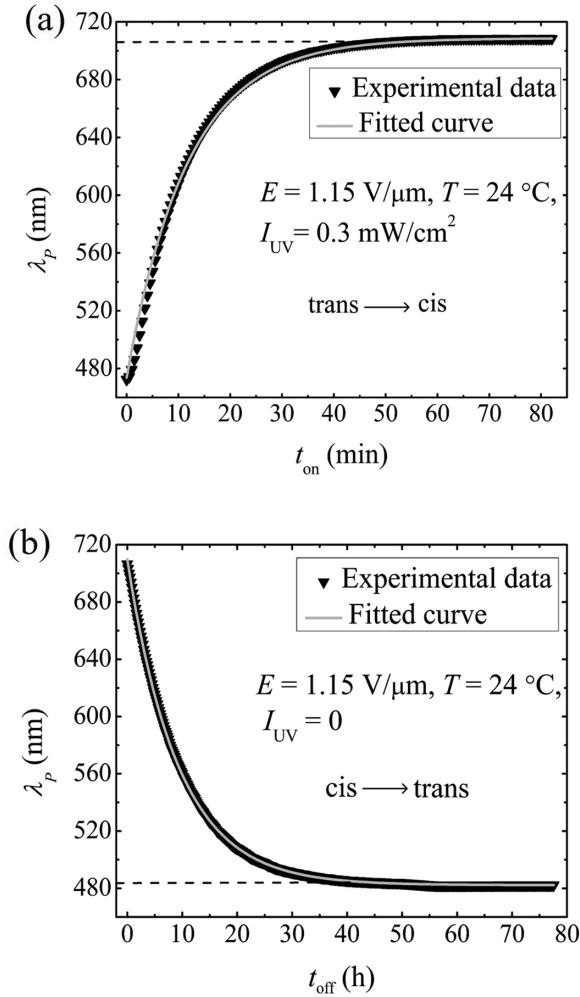


FIG. 4. Dynamics of the peak wavelength  $\lambda_p$  shifts in the hybrid  $\text{ChOH}$  cell with thickness  $d = (9.25 \pm 0.02) \mu\text{m}$  at a constant electric field  $E = 1.15 \text{ V}/\mu\text{m}$ : (a)  $\lambda_p$  as a function of the UV exposure time  $t_{\text{on}}$  for UV irradiation at 365 nm,  $0.3 \text{ mW}/\text{cm}^2$ ; (b)  $\lambda_p$  as a function of the relaxation time  $t_{\text{off}}$  after UV is switched off.

at the same temperature,  $T = 24.0^\circ\text{C}$ , under a fixed electric field of the rms amplitude  $E = 1.15 \text{ V}/\mu\text{m}$ . Note that this field causes reflection at a relatively short wavelength 473 nm. The reason for this choice is that the UV irradiation produces a redshift of the Bragg reflection band, as described below; the chosen field keeps the redshifted reflection in the visible part of the spectrum to facilitate characterization and analysis. Experiments with other electric field values and other chemical compositions of the mixtures produce qualitatively similar results and will not be discussed here.

Continuous irradiation with unpolarized UV light ( $\lambda = 365 \text{ nm}$ ) of low intensity ( $I_{\text{UV}} = 0.3 \text{ mW}/\text{cm}^2$ ) causes a continuous redshift of the reflection wavelength from  $\lambda_p^o = 473 \text{ nm}$  to  $\lambda_p^{\text{on}} = 708 \text{ nm}$  after 1.5 h of irradiation, Fig. 4(a). The redshift starts to saturate after about 40 min of UV irradiation. Once the UV is switched off,  $\lambda_p$  gradually relaxes back to the shorter values, at a rate that is much slower than the redshift rate under the UV, coming close to the initial pre-UV wavelength of 473 nm, but remaining a few nm above it even

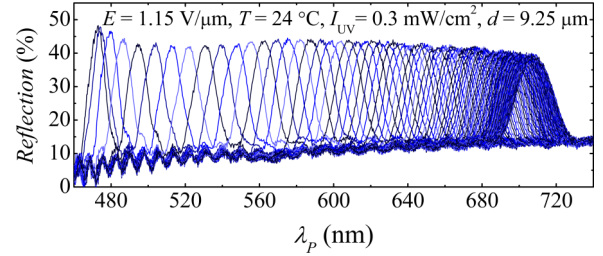


FIG. 5. Bragg reflection spectra during 1.5 h of UV irradiation 365 nm,  $0.3 \text{ mW}/\text{cm}^2$  recorded every 30 s at the planar side of the hybrid  $\text{ChOH}$  cell with thickness  $d = (9.25 \pm 0.02) \mu\text{m}$  at fixed temperature  $T = 24.0^\circ\text{C}$  and electric field  $E = 1.15 \text{ V}/\mu\text{m}$ . The UV irradiation causes a redshift of the reflection band.

after 80 h; see Fig. 4(b). This slow relaxation is a common property of azo- and azoxybenzene compounds [16,49].

The dependence of  $\lambda_p$  on the duration  $t_{\text{on}}$  of UV irradiation in Fig. 4(a) is well fitted by an exponential dependence,

$$\lambda_p(t_{\text{on}} \geq 0) = \lambda_p^{\text{on}} + (\lambda_p^o - \lambda_p^{\text{on}})e^{-\frac{t_{\text{on}}}{\tau_{\text{on}}}}, \quad (4)$$

where  $t_{\text{on}}$  is the UV exposure time measured from the moment the UV irradiation is switched on;  $\lambda_p^o = 473 \text{ nm}$  and  $\lambda_p^{\text{on}} = 708 \text{ nm}$  are the stationary peak wavelengths when UV is off and on, respectively; and the fitting parameter  $\tau_{\text{on}} = 11.7 \text{ min}$  is the characteristic time of the  $\text{ChOH}$  reflection wavelength response to the continuous UV irradiation. Similarly, the blueshift during the relaxation, Fig. 4(b), is well described by

$$\lambda_p(t_{\text{off}} \geq 0) = \lambda_p^{\text{off}} + (\lambda_p^{\text{on}} - \lambda_p^{\text{off}})e^{-\frac{t_{\text{off}}}{\tau_{\text{off}}}}, \quad (5)$$

where  $t_{\text{off}}$  is the time measured from the moment the UV irradiation is switched off,  $\tau_{\text{off}} = 9.25 \text{ h}$  is the fitted value of the relaxation characteristic time, and  $\lambda_p^{\text{off}} = 482 \text{ nm}$  is the peak wavelength at the stationary relaxed state in the dark.

The redshift of reflection spectra over the entire 1.5 h of UV irradiation corresponding to each value of the experimental data points of Fig. 4(a) is shown in Fig. 5. The time interval between each reflection spectrum is 30 s. Note that the efficiency of reflection decreases in the red and near-infrared regions. One reason is that the pitch increase implies that the Bragg reflection is less effective since it involves a smaller number of  $\text{ChOH}$  pseudolayers. The second reason is that as the UV irradiation progresses with time and more *cis* isomers form, the structure becomes slightly nonuniform, as evidenced by textural observation discussed below.

The three different colors reflected by the planar side of the hybrid  $\text{ChOH}$  cell at the beginning of UV exposure,  $t_{\text{on}} = 0 \text{ min}$ , and during the exposure,  $t_{\text{on}} = 4.4 \text{ min}$  and  $t_{\text{on}} = 11.6 \text{ min}$  of continuous UV irradiation, are shown in Figs. 6(a)–6(c), respectively. The change of the pitch often involves the formation of slow-relaxing defects, such as edge dislocations, as described previously for both Ch [50] and  $\text{ChOH}$  [7,47] structures. These metastable defects cause some light scattering and small variations of the structural colors within the plane of the cell; some of these can be seen in Fig. 6(c). Nonuniformity of the samples after a prolonged UV exposure and decrease in the number of pseudolayers explain the decrease of reflection efficiency observed in the red and near-infrared part of the spectra in Fig. 5.



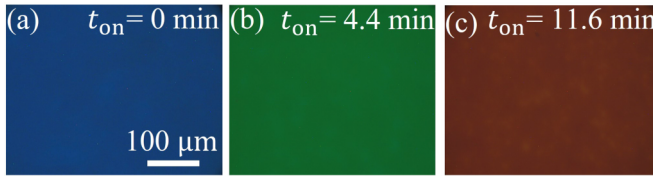


FIG. 6. (a) Blue, (b) green, and (c) red colors reflected by the planar side of the hybrid  $\text{Ch}_{\text{OH}}$  cell with thickness  $d = (9.25 \pm 0.02) \mu\text{m}$  at fixed temperature  $T = 24.0^\circ\text{C}$  and electric field  $E = 1.15 \text{ V}/\mu\text{m}$  at three different instances of UV irradiation  $365 \text{ nm}$ ,  $0.3 \text{ mW}/\text{cm}^2$ .

There are two potential reasons for the redshift of the reflection peak during UV irradiation: (1) heating of the cell caused by both UV and the electric field and (2) UV photoisomerization of D7AOB molecules. The  $\text{Ch}_{\text{OH}}$  state is indeed temperature sensitive, but this sensitivity cannot explain the effects presented in Figs. 4–6. To demonstrate this, we measured the temperature dependence of the peak wavelength  $\lambda_p$ ; see Fig. 7, which shows that the reflection peak wavelength increases monotonously with the increase in temperature, at the rate of  $55 \text{ nm}/^\circ\text{C}$ . However, the direct measurement of sample temperature by the thermocouple for 1 h during UV irradiation at a constant electric field indicates that the temperature changes are smaller than  $0.01^\circ\text{C}$ . If there is no UV irradiation, the temperature of the cell under a continuous electric field activation varied by  $0.27^\circ\text{C}$  over a 35 h period of observation; this change is most likely caused by fluctuations in the room temperature. Even with the over-estimated temperature change of  $0.27^\circ\text{C}$ , the spectral shift would be about  $15 \text{ nm}$ , much smaller than the observed  $235 \text{ nm}$  shifts in Fig. 4(a). Therefore, the thermally induced shift of the reflection wavelength is negligibly small as compared to the UV-induced shifts in Fig. 4(a). Furthermore, the idea that the wavelength shift could be caused by the electric field heating is also contradicted by the experimental data in Fig. 4(a), since the characteristic time of electric field heating effects is  $\sim 1 \text{ s}$  [51], while the experiment shows a much longer

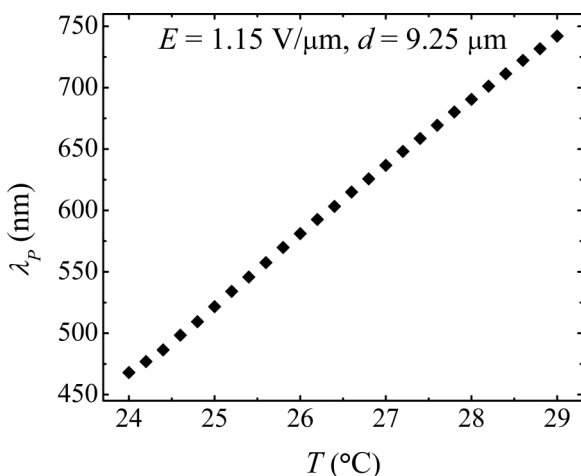


FIG. 7. Temperature dependence of the reflection peak  $\lambda_p$  at a constant electric field  $E = 1.15 \text{ V}/\mu\text{m}$  in a  $\text{Ch}_{\text{OH}}$  cell with  $d = (9.25 \pm 0.02) \mu\text{m}$ .

time,  $\tau_{\text{on}} \sim 12 \text{ min}$ . Note here that we do not exclude the possibility of some temperature increase by UV irradiation, but this thermal effect is expected to be of the same short characteristic time as the heating effects caused by the electric field; it does not influence the dynamics on the time scales of  $\tau_{\text{on}}$ . We conclude that the spectral shifts caused by switching the UV irradiation on and off are caused primarily by the photoisomerization of D7AOB.

UV irradiation causes a shift in the phase transition temperatures. After 1.5 h of continuous UV irradiation,  $T_{N^*-N_{\text{TB}}}$  of the chiral mixture decreases by  $2.8^\circ\text{C}$  and  $T_{N-N_{\text{TB}}}$  of the nonchiral mixture decreases by  $3.2^\circ\text{C}$ . There is no effect of UV on the clearing temperatures  $T_{I-N^*}$  and  $T_{I-N}$ , apparently, because heating facilitates *cis*-to-*trans* isomerization [38]. These changes should be attributed to modifications of the molecular interactions triggered by the appearance of the *cis* isomers of D7AOB. Discussion of light-induced effects in liquid crystals caused by *trans*-*cis* isomerization usually ends at the statement that the isomers somehow change the molecular interactions. The unique structure of  $\text{Ch}_{\text{OH}}$  allows us to explore the mechanism at a deeper level and connect it to the concrete material parameter, namely, to show that the UV irradiation causes an increase of the bend elastic constant, as described below.

At first sight, Eqs. (1)–(3) suggest that the UV effect might in principle be rooted in the changes of many parameters, such as two refractive indices  $n_o$  and  $n_e$ , the conical angle  $\theta$ , dielectric anisotropy  $\Delta\epsilon$ , and the bend elastic constant  $K_{33}$ . We first analyze how much the UV-induced isomerization could change the refractive indices of the mixture.

*Effect of UV on the refractive indices.* Before the UV exposure,  $n_o = 1.519$ ,  $n_e = 1.726$ ,  $\Delta n = 0.207$ , and  $(n_o + n_e)/2 = 1.623$ , as measured at  $532 \text{ nm}$ , and  $T = T_{N-N_{\text{TB}}} + 2.0^\circ\text{C} = 21.4^\circ\text{C}$ . After 1.5 h of continuous UV exposure, these values change very little:  $n_o = 1.522$ ,  $n_e = 1.728$ ,  $\Delta n = 0.206$ , and  $(n_o + n_e)/2 = 1.625$ , indicating that the dramatic shift of  $\lambda_p$  cannot be attributed to the UV-induced change of the refractive indices in Eq. (3). Furthermore, the data on the refractive indices exclude any role of the conical tilt angle  $\theta$  in the redshift of the Bragg peaks under UV, as discussed in detail below.

*Absence of the conical angle effect on redshift.* According to Eq. (3), the reflection wavelength depends on the average refraction index  $\bar{n}_{\text{eff}} = (n_o + n_{e,\text{eff}})/2$ , where the effective extraordinary index  $n_{e,\text{eff}} = n_o n_e / \sqrt{n_e^2 \cos^2 \theta + n_o^2 \sin^2 \theta}$  is a function of  $\theta$  and thus of the electric field  $E$ ; see Eq. (2). As shown theoretically and experimentally in Ref. [7], the conical angle  $\theta$  could not exceed about  $30^\circ$  since at a larger  $\theta$  the  $\text{Ch}_{\text{OH}}$  state transforms into a conventional right-angle Ch. Suppose that the redshift of Bragg spectra is caused by the change of  $\theta$ , from a hypothetical grossly underestimated value of  $0^\circ$  in the dark to the maximum  $30^\circ$  under UV. Then  $\bar{n}_{\text{eff}} = n_o = 1.519$  for  $\theta = 0^\circ$  and  $\bar{n}_{\text{eff}} = 1.544$  for  $\theta = 30^\circ$ . This change by  $0.025$  represents only about  $1.6\%$  of  $\bar{n}_{\text{eff}}$  and thus cannot explain the shift of the Bragg wavelength by  $50\%$ , from  $473$  to  $708 \text{ nm}$ ; see Fig. 4. More evidence that the change in conical angle could not be responsible for the observed redshift comes from the expression  $\bar{n}_{\text{eff}} = n_o [1 + \frac{1}{4} (1 - \frac{n_e^2}{n_o^2}) \sin^2 \theta]$ , valid for small  $\theta$  [41]. With the

measured refractive indices, the factor  $\frac{1}{4}(1 - \frac{n_o^2}{n_e^2})$  is very small, 0.056. Therefore, even if  $\theta$  varies within an exaggerated range  $0^\circ - 30^\circ$ , it could not cause a change in the optical factor  $\bar{n}_{\text{eff}}$  by more than 3%. A similar absence of the  $\theta$  effect was established for field dependencies of the Bragg wavelength in Ref. [41].

**Anisotropy of dielectric permittivity.** The dielectric anisotropy  $\Delta\epsilon$  measured in a planar cell of the thickness  $(4.66 \pm 0.01) \mu\text{m}$  at temperature  $T = 24^\circ\text{C}$  before the UV exposure and after 1.5 h of continuous UV irradiation at 365 nm,  $0.3 \text{ mW}/\text{cm}^2$ , is found to be 7.18 and 6.90, respectively. The UV-induced decrease of  $\Delta\epsilon$  is 0.28, or 4%, too small to explain the spectral shifts. Note here that Lisetski *et al.* [52] presented similar direct evidence of the UV-induced weakening of dielectric anisotropy in azoxybenzene nematics.

**Bend elastic constant.**  $K_{33}$  is calculated from the dependency  $\lambda_P/n_o(\lambda_P) = a_1 E^{-1} + a_2 E^{-2}$ , as described in the Materials and Methods section and Ref. [41], using a hybrid aligned cell of the thickness  $d = (9.25 \pm 0.02) \mu\text{m}$  at a fixed temperature  $T = 24^\circ\text{C}$ . Before the UV exposure,  $n_o = 1.528$ , 1.519, and 1.509 at 488, 532, and 632.8 nm, respectively. These values of  $n_o$  are extrapolated by the Cauchy dispersion relation  $n_o(\lambda) = A + B\lambda^{-2} + C\lambda^{-4}$ , with  $A = 1.505$ ,  $B = -4.038 \times 10^{-3} \mu\text{m}^2$ , and  $C = 2.270 \times 10^{-3} \mu\text{m}^4$ . The dependence  $\lambda_P/n_o(\lambda_P)$  vs  $E^{-1}$  is strictly linear, Fig. 8(a), which implies that its slope  $a_1$  could be used to determine  $K_{33} = \epsilon_o \Delta\epsilon a_1^2 / 4\pi^2$  as  $K_{33} = 0.19 \text{ pN}$ . After 1.5 h of continuous UV irradiation, the values of  $n_o$  are 1.529, 1.522, and 1.513 at 488, 532, and 632.8 nm, respectively, yielding  $A = 1.501$ ,  $B = 2.220 \times 10^{-3} \mu\text{m}^2$ ,  $C = 1.073 \times 10^{-3} \mu\text{m}^4$ , and a dramatically higher  $K_{33} = 0.42 \text{ pN}$ , Fig. 8(b). The linear character of  $\lambda_P/n_o(\lambda_P)$  vs  $E^{-1}$  provides additional evidence that the possible UV modification of the conical angle  $\theta$  is not affecting the Bragg spectra, as the field dependence of  $\theta$  enters the expression for the term  $a_2 E^{-2}$ , which is about two orders of magnitude smaller than the linear term  $a_1 E^{-1}$  [41]. We conclude that the main effect of UV irradiation is a dramatic increase of  $K_{33}$  by a factor larger than 2, from 0.19 pN in the dark to 0.42 pN after 1.5 h of continuous exposure. This increase of  $K_{33}$  is the main reason for the redshift of Bragg spectra under UV irradiation.

As established above, UV irradiation causes a small decrease in dielectric anisotropy, temperatures  $T_{N^* - N_{\text{TB}}}$ , and  $T_{N - N_{\text{TB}}}$ . These changes could be treated as the effective temperature increase and the associated decrease of the scalar order parameter, which is natural since *cis* isomers disrupt the parallel alignment of neighboring molecules. The most important point is that the *trans*-to-*cis* isomerization dramatically increases the bend elastic constant  $K_{33}$ . It is known that the bend elastic constant  $K_{33}$  in the flexible dimer nematics and cholesterics shows a complicated nonmonotonous behavior as a function of temperature [40,41]. Upon cooling from the isotropic phase,  $K_{33}$  first increases and then decreases, reaching a minimum at about  $1^\circ\text{C}$  above the transition into the twist-bend state [40,41]. Experiments by Aronzon *et al.* [38] show that UV generation of *cis* isomers in azoxybenzenes reduces the scalar order parameter and birefringence, a behavior that mimics the effect of heating. Since  $K_{33}$  increases upon heating when one moves sufficiently far away from the  $N_{\text{TB}}$

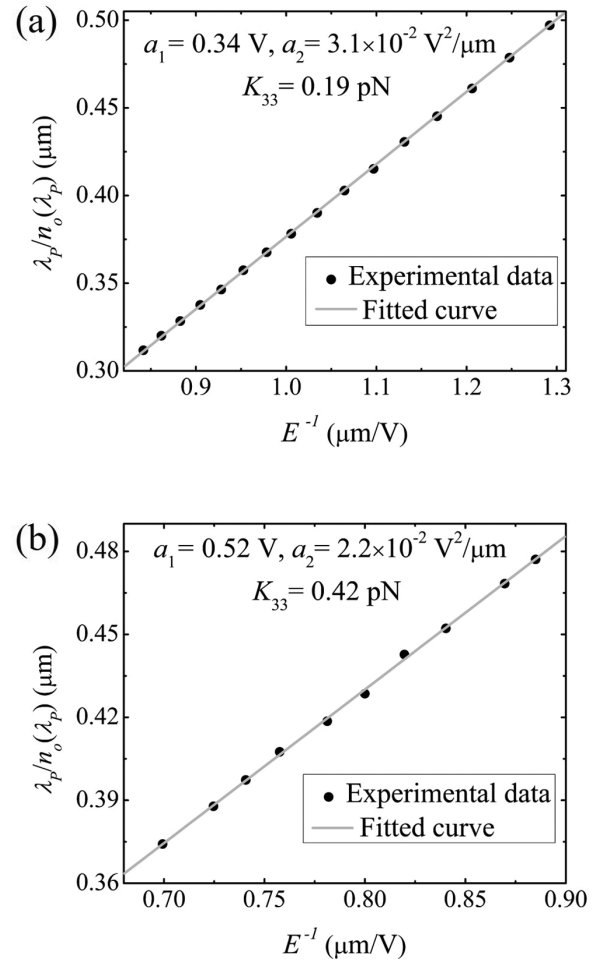


FIG. 8. Dependencies  $\lambda_P/n_o(\lambda_P)$  vs  $E^{-1}$  fitted with a polynomial  $a_1 E^{-1} + a_2 E^{-2}$  and the calculated bend elastic constant (a)  $K_{33} = 0.19 \text{ pN}$  before UV irradiation and (b)  $K_{33} = 0.42 \text{ pN}$  after 1.5 h of continuous UV irradiation.

phase, the increase of  $K_{33}$  by *trans-cis* isomerization is linked to the reduced scalar order parameter. The increase of  $K_{33}$  results in the increase of the  $\text{Ch}_{\text{OH}}$  pitch  $P \propto \sqrt{K_{33}/\Delta\epsilon}$ , which explains the UV-induced redshift of the reflection wavelength  $\lambda_P$ . In the next section, we present a kinetic model of the UV effect in order to substantiate the exponential processes revealed by the fitting of the experimental data, Eqs. (4) and (5).

The sensitivity of the structure to UV irradiation is remarkably strong. The concentration of D7AOB in the mixture is 10 wt %. The maximum concentration of *cis* isomers created by UV irradiation at 365 nm is expected to be 50% [38]; thus the observed spectral shift of  $\lambda_P$  by about 235 nm is triggered by transformations of only about 5 wt % of all the molecules in the mixture. Usually, the mechanisms of the UV-induced changes in liquid crystals doped with azoxybenzenes and azobenzenes are associated with the fact that the rodlike *trans* isomers fit well in the orientationally ordered environment, while the *cis* isomers do not [11–16,18,38,49,53]. In the case of photosensitive conventional Ch, isomerization transitions of photosensitive achiral dopants such as D7AOB change both the intrinsic (field-free) pitch  $P_o$  and the refractive indices,

although the detailed molecular mechanisms remain difficult to uncover [11]. The peculiar properties of  $\text{Ch}_{\text{OH}}$  allow one to draw a concrete connection between the material properties such as the bend elastic constant and photoisomerization.

#### IV. KINETIC MODEL OF *TRANS-CIS* PHOTOISOMERIZATION

The kinetic model of *trans-cis* photoisomerization explains the experimentally observed temporal behavior of the reflection peak and hence the fitted equations (4) and (5). The photoisomerization of D7AOB is modeled by the standard kinetic equations that control the dynamics of transitions between *trans* and *cis* isomers [54].

Under the irradiation by a monochromatic source with intensity  $I(\lambda_{\text{irr}}, t)$  at the wavelength  $\lambda_{\text{irr}}$ , the relative concentrations of D7AOB molecules in the *trans* state  $n_t(t)$  and in the *cis* state  $n_c(t)$  obey the following kinetic equations,

$$\begin{aligned} dn_c(t)/dt &= -k(t)n_c(t) + k'(t)n_t(t), \\ dn_t(t)/dt &= k(t)n_c(t) - k'(t)n_t(t), \end{aligned} \quad (6)$$

where  $k'(t) = A' + B'(\lambda_{\text{irr}})I(\lambda_{\text{irr}}, t)$  and  $k(t) = A + B(\lambda_{\text{irr}})I(\lambda_{\text{irr}}, t)$  are the transition rates from *trans* to *cis* isomer and vice versa, respectively;  $A'$  and  $A$  are the transition rates without irradiation;  $B'(\lambda_{\text{irr}})$  and  $B(\lambda_{\text{irr}})$  are the photoisomerization coefficients [55]. For azoxybenzene derivatives, such as D7AOB,  $B'(\lambda_{\text{irr}})$  and  $B(\lambda_{\text{irr}})$  exhibit a strong dispersion, resulting in  $B'(\lambda_{\text{irr}}) > B(\lambda_{\text{irr}})$  for UV irradiation, but  $B'(\lambda_{\text{irr}}) < B(\lambda_{\text{irr}})$  for irradiation in the visible range. Thus, for a broadband irradiation source,  $k'(t)$  and  $k(t)$  should contain integrals over  $\lambda_{\text{irr}}$ .

Equations (6) obey the conservation law,  $n_t(t) + n_c(t) = 1$ , and can be reduced to

$$\frac{dn_c(t)}{dt} = k'(t) - [k'(t) + k(t)]n_c(t). \quad (7)$$

When the irradiation is of a constant intensity or absent, both  $k'(t)$  and  $k(t)$  are constants, and Eq. (7) has the solution

$$n_c(t > t_0) = \bar{n}_c + [n_c(t_0) - \bar{n}_c]e^{-(k+k')t}, \quad (8)$$

where  $t_0$  can be any time moment provided the intensity is constant and  $\bar{n}_c = k/(k' + k)$  is the stationary relative concentration of the *cis* molecules that establishes itself after a sufficiently long time  $t - t_0 \gg \tau = (k' + k)^{-1}$ . When the irradiation is off,  $\bar{n}_c = \bar{n}_c^{\text{off}} = A'/(A' + A)$  and  $\tau_{\text{off}} = (A' + A)^{-1}$ , and when the irradiation is on,  $\bar{n}_c = \bar{n}_c^{\text{on}} = (A' + B'I)/(A' + A + (B' + B)I)$  and  $\tau_{\text{on}} = [A' + A + (B' + B)I]^{-1}$ . We assume proportionality between the photoinduced shift of Bragg reflection peak  $\lambda_P - \lambda_P^{\text{off}}$  and the photoinduced change of the relative concentration of *cis* molecules  $n_c(t) - \bar{n}_c^{\text{off}}$  [11],

$$\lambda_P - \lambda_P^{\text{off}} = K[n_c(t) - \bar{n}_c^{\text{off}}], \quad (9)$$

where  $K$  is a positive proportionality constant. Now, the fitted equations (4) and (5) can be combined as

$$\lambda_P(t > t_0) = \bar{\lambda}_P + [\lambda_P(t_0) - \bar{\lambda}_P]e^{-\frac{t}{\tau}}, \quad (10)$$

The experiment explores two regimes:

(1) continuous UV irradiation with  $\tau_{\text{on}} = [A' + A + (B' + B)I_{\text{UV}}]^{-1} = 11.7$  min,  $\lambda_P(t_0) = \lambda_P(0) = \lambda_P^{\text{on}} = 473$  nm and  $\bar{\lambda}_P = \lambda_P^{\text{on}} = 708$  nm;

(2) relaxation in the dark after UV radiation is switched off, with  $\tau_{\text{off}} = (A' + A)^{-1} = 9.25$  h,  $\lambda_P(t_0) = \lambda_P(0) = \lambda_P^{\text{on}} = 708$  nm, and  $\bar{\lambda}_P = \lambda_P^{\text{off}} = 482$  nm.

This model (9) explains the dynamics of  $\lambda_P$  by connecting the spectral changes to the instantaneous concentration of molecules in the *cis* state. Because of the difference in the characteristic times, the thermal relaxation process can easily be neglected during the UV photoisomerization:  $A + A' \ll I_{\text{UV}}(B + B')$ .

#### V. CONCLUSION

Our study demonstrates that the pitch of the oblique helical cholesteric can be tuned by simultaneous action of the electric field and low-intensity UV irradiation. Light irradiation that causes molecular isomerization is another powerful control parameter to tune the pitch and diffractive properties of  $\text{Ch}_{\text{OH}}$ , adding to the list that already includes static electric [7,8] and magnetic [9] fields, optical torques [10], composition, and temperature [8,47]. The underlying principle is *trans-cis* photoisomerization of an achiral azoxybenzene dopant, the dynamics of which is described by a kinetic model. Direct measurements of the material parameters show that the *trans-to-cis* photoisomerization mainly causes the increase of the bend elastic constant  $K_{33}$ . This effect explains the experimentally observed redshift of  $\text{Ch}_{\text{OH}}$  reflection spectra under UV irradiation. The increase of  $K_{33}$  is associated with the fact that *trans-to-cis* photoisomerization leads to a decrease of transition temperature from the cholesteric (or nematic) to the twist-bend nematic phase, mimicking the heating effect and the associated decrease of the scalar order parameter.  $K_{33}$  in flexible dimer liquid crystals is known to show a nonmonotonous dependence on temperature; thus the increase of  $K_{33}$  under UV irradiation could be explained by the decreased scalar order parameter. The change in molecular curvature of the D7AOB molecule during *trans-to-cis* photoisomerization might also contribute to the increase of  $K_{33}$  [56]. The sensitivity of the  $\text{Ch}_{\text{OH}}$  to the UV irradiation is extraordinarily strong, as the spectral shift of the Bragg reflection maximum by about 235 nm is achieved by photoisomerization of only about 5 wt% of achiral molecules in the mixture. The sensitivity could be further increased if the photosensitive functionality is assigned to the chiral azodopant [16,29–31]. Hybrid surface anchoring allows one to change the pitch and thus the wavelength of selective reflection or transmission of light in a continuous manner.

The presented proof of concept of the phototunable  $\text{Ch}_{\text{OH}}$  structures is demonstrated with the azoxybenzene derivative D7AOB. The azoxybenzene compounds such as this one show a relatively slow relaxation when the UV is switched off. In practical applications that require a faster response, one can use other photosensitive materials with a quicker response [57,58] and a wide tunable range [16,57]. In the explored case, the UV irradiation was of fixed intensity. It would be of interest to explore whether the variable intensity of irradiation could be used to dynamically control the rate of the



wavelength shifts. Photo-electro optical effects in  $\text{Ch}_{\text{OH}}$  could be improved further by using flexible dimers that are photo-sensitive [59], and photosensitive chiral dopants [29–31]. This work is in progress.

## ACKNOWLEDGMENTS

The work was supported by the National Science Foundation Grant No. ECCS-1906104. We thank Dr. Hao Wang for help with Fig. 1.

- 
- [1] D.-K. Yang and S.-T. Wu, *Fundamentals of Liquid Crystal Devices* (John Wiley & Sons, Chichester, UK, 2006), p. 394.
- [2] P. G. de Gennes, *Solid State Commun.* **6**, 163 (1968).
- [3] R. B. Meyer, *Appl. Phys. Lett.* **12**, 281 (1968).
- [4] D. Subacius, S. V. Shiyonovskii, Ph. Bos, and O. D. Lavrentovich, *Appl. Phys. Lett.* **71**, 3323 (1997).
- [5] S. V. Shiyonovskii, D. Voloschenko, T. Ishikawa, and O. D. Lavrentovich, *Mol. Cryst. Liq. Cryst.* **358**, 225 (2001).
- [6] H. Q. Xianyu, S. Faris, and G. P. Crawford, *Appl. Opt.* **43**, 5006 (2004).
- [7] J. Xiang, S. V. Shiyonovskii, C. T. Imrie, and O. D. Lavrentovich, *Phys. Rev. Lett.* **112**, 217801 (2014).
- [8] J. Xiang, Y. N. Li, Q. Li, D. A. Paterson, J. M. D. Storey, C. T. Imrie, and O. D. Lavrentovich, *Adv. Mater.* **27**, 3014 (2015).
- [9] S. M. Salili, J. Xiang, H. Wang, Q. Li, D. A. Paterson, J. M. D. Storey, C. T. Imrie, O. D. Lavrentovich, S. N. Sprunt, J. T. Gleeson, and A. Jákli, *Phys. Rev. E* **94**, 042705 (2016).
- [10] G. Nava, F. Ciciulla, O. S. Iadlovská, O. D. Lavrentovich, F. Simoni, and L. Lucchetti, *Phys. Rev. Res.* **1**, 033215 (2019).
- [11] E. Sackmann, *J. Am. Chem. Soc.* **93**, 7088 (1971).
- [12] V. Vinogradov, A. Khizhnyak, L. Kutulya, Yu. A. Reznikov, and V. Reshetnyak, *Mol. Cryst. Liq. Cryst.* **192**, 273 (1990).
- [13] S. Kurihara, T. Kanda, T. Nagase, and T. Nonaka, *Appl. Phys. Lett.* **73**, 2081 (1998).
- [14] S. V. Serak, E. O. Arikainen, H. F. Gleeson, V. A. Grozhik, J.-P. Guillou, and N. A. Usova, *Liq. Cryst.* **29**, 19 (2002).
- [15] U. A. Hrozhyk, S. V. Serak, N. V. Tabiryan, and T. J. Bunning, *Adv. Funct. Mater.* **17**, 1735 (2007).
- [16] T. J. White, R. L. Bricker, L. V. Natarajan, N. V. Tabiryan, L. Green, Q. Li, and T. J. Bunning, *Adv. Funct. Mater.* **19**, 3484 (2009).
- [17] T. J. White, A. S. Freer, N. V. Tabiryan, and T. J. Bunning, *J. Appl. Phys.* **107**, 073110 (2010).
- [18] Y. Wang and Q. Li, *Adv. Mater.* **24**, 1926 (2012).
- [19] A. Chanishvili, G. Chilaya, G. Petriashvili, and D. Sikharulidze, *Mol. Cryst. Liq. Cryst.* **409**, 209 (2004).
- [20] G. Chilaya, A. Chanishvili, G. Petriashvili, R. Barberi, R. Bartolino, M. P. De Santo, M. A. Matranga, and P. Collings, *Mol. Cryst. Liq. Cryst.* **453**, 123 (2006).
- [21] G. Chilaya, A. Chanishvili, G. Petriashvili, R. Barberi, R. Bartolino, G. Cipparrone, A. Mazzulla, and P. V. Shibaev, *Adv. Mater.* **19**, 565 (2007).
- [22] U. A. Hrozhyk, S. V. Serak, N. V. Tabiryan, and T. J. Bunning, *Adv. Mater.* **19**, 3244 (2007).
- [23] M. Aronishidze, A. Chanishvili, G. Chilaya, G. Petriashvili, S. Tavzarashvili, L. Lisetski, I. Gvozдовskyy, and I. Terenetskaya, *Mol. Cryst. Liq. Cryst.* **420**, 47 (2004).
- [24] T. Yamaguchi, T. Inagawa, H. Nakazumi, S. Irie, and M. Irie, *Mol. Cryst. Liq. Cryst.* **365**, 1817 (2001).
- [25] T. Yamaguchi, T. Inagawa, H. Nakazumi, S. Irie, and M. Irie, *J. Mater. Chem.* **11**, 2453 (2001).
- [26] S. Pieraccini, S. Masiero, G. P. Spada, and G. Gottarelli, *Chem. Commun.* **5**, 598 (2003).
- [27] S. Pieraccini, G. Gottarelli, R. Labruto, S. Masiero, O. Pandoli, and G. P. Spada, *Chem. - Eur. J.* **10**, 5632 (2004).
- [28] Q. Li, L. Green, N. Venkataraman, I. Shiyonovskaya, A. Khan, A. Urbas, and J. W. Doane, *J. Am. Chem. Soc.* **129**, 12908 (2007).
- [29] H. Wang, H. K. Bisoyi, M. E. McConney, A. M. Urbas, T. J. Bunning, and Q. Li, *Adv. Mater.* **31**, 1902958 (2019).
- [30] H. Wang, H. K. Bisoyi, A. M. Urbas, T. J. Bunning, and Q. Li, *J. Am. Chem. Soc.* **141**, 8078 (2019).
- [31] H. Wang, H. K. Bisoyi, B.-X. Li, M. E. McConney, T. J. Bunning, and Q. Li, *Angew. Chem., Int. Ed.* **59**, 2684 (2020).
- [32] L. Wang and Q. Li, *Chem. Soc. Rev.* **47**, 1044 (2018).
- [33] R. S. Zola, H. K. Bisoyi, H. Wang, A. M. Urbas, T. J. Bunning, and Q. Li, *Adv. Mater.* **31**, 1806172 (2019).
- [34] M. E. McConney, M. Rumi, N. P. Godman, U. N. Tohgha, and T. J. Bunning, *Adv. Opt. Mater.* **7**, 1900429 (2019).
- [35] A. Y.-G. Fuh, S.-J. Ho, S.-T. Wu, and M.-S. Li, *Appl. Opt.* **53**, 1658 (2014).
- [36] J.-D. Lin, M.-H. Hsieh, G.-J. Wei, T.-S. Mo, S.-Y. Huang, and C.-R. Lee, *Opt. Express* **21**, 15765 (2013).
- [37] N. C. Davy, M. Sezen-Edmonds, J. Gao, X. Lin, A. Liu, N. Yao, A. Kahn, and Y.-L. Loo, *Nat. Energy* **2**, 17104 (2017).
- [38] D. Aronzon, E. P. Levy, P. J. Collings, A. Chanishvili, G. Chilaya, and G. Petriashvili, *Liq. Cryst.* **34**, 707 (2007).
- [39] W. R. Folks, Yu. A. Reznikov, S. Yarmolenko, and O. Lavrentovich, *Mol. Cryst. Liq. Cryst. Sci. Technol., Sect. A* **292**, 183 (1997).
- [40] G. Babakhanova, Z. Parsouzi, S. Paladugu, H. Wang, Yu. A. Nastishin, S. V. Shiyonovskii, S. Sprunt, and O. D. Lavrentovich, *Phys. Rev. E* **96**, 062704 (2017).
- [41] O. S. Iadlovská, G. Babakhanova, G. H. Mehl, C. Welch, E. Cruickshank, G. J. Strachan, J. M. D. Storey, C. T. Imrie, S. V. Shiyonovskii, and O. D. Lavrentovich, *Phys. Rev. Res.* **2**, 013248 (2020).
- [42] J. van der Veen, W. H. de Jeu, A. H. Grobber, and J. Boven, *Mol. Cryst. Liq. Cryst.* **17**, 291 (1972).
- [43] W. H. de Jeu, Th. W. Lathouwers, and P. Bordewijk, *Phys. Rev. Lett.* **32**, 40 (1974).
- [44] W. H. de Jeu and W. A. P. Claassen, *J. Chem. Phys.* **67**, 3705 (1977).
- [45] J. Kędzierski, Z. Raszewski, M. Kojdecki, E. Kruszelnicki-Nowinowski, P. Perkowski, W. Piecek, E. Miszczyk, J. Zieliński, P. Morawiak, and K. Ogrodnik, *Opto-Electron. Rev.* **18**, 214 (2010).
- [46] O. S. Iadlovská, G. R. Maxwell, G. Babakhanova, G. H. Mehl, C. Welch, S. V. Shiyonovskii, and O. D. Lavrentovich, *Opt. Lett.* **43**, 1850 (2018).
- [47] M. Mrukiewicz, O. S. Iadlovská, G. Babakhanova, S. Siemianowski, S. V. Shiyonovskii, and O. D. Lavrentovich, *Liq. Cryst.* **46**, 1544 (2019).



- [48] O. D. Lavrentovich, *Opt. Mater. Express* **10**, 2415 (2020).
- [49] W. R. Folks, S. Keast, T. A. Krentzel, B. Zalar, H. Zeng, Yu. A. Reznikov, M. Neubert, S. Kumar, D. Finotello, and O. D. Lavrentovich, *Mol. Cryst. Liq. Cryst. Sci. Technol., Sect. A* **320**, 77 (1998).
- [50] I. I. Smalyukh and O. D. Lavrentovich, *Phys. Rev. E* **66**, 051703 (2002).
- [51] Y. Yin, S. V. Shiyanovskii, and O. D. Lavrentovich, *J. Appl. Phys.* **100**, 024906 (2006).
- [52] L. N. Lisetski, A. N. Samoilov, S. S. Minenko, A. P. Fedoryako, and T. V. Bidna, *Funct. Mater.* **25**, 681 (2018).
- [53] Y. Lansac, M. A. Glaser, N. A. Clark, and O. D. Lavrentovich, *Nature (London)* **398**, 54 (1999).
- [54] P. Atkins, J. de Paula, and J. Keeler, *Atkins' Physical Chemistry* (Oxford University Press, Oxford, 2018).
- [55] P. Arya, J. Jelken, N. Lomadze, S. Santer, and M. Bekir, *J. Chem. Phys.* **152**, 024904 (2020).
- [56] A. Jákli, O. D. Lavrentovich, and J. V. Selinger, *Rev. Mod. Phys.* **90**, 045004 (2018).
- [57] T. J. White, S. A. Cazzell, A. S. Freer, D.-K. Yang, L. Sukhomlinova, L. L. Su, T. Kosa, B. Taheri, and T. J. Bunning, *Adv. Mater.* **23**, 1389 (2011).
- [58] T. V. Mykytiuk, I. P. Ilchishin, O. V. Yaroshchuk, R. M. Kravchuk, Y. Li, and Q. Li, *Opt. Lett.* **39**, 6490 (2014).
- [59] D. A. Paterson, J. Xiang, G. Singh, R. Walker, D. M. Agra-Kooijman, A. Martnez-Felipe, M. Gao, J. M. D. Storey, S. Kumar, O. D. Lavrentovic *et al.*, *J. Am. Chem. Soc.* **138**, 5283 (2016).